Qinlan Li
State Key Laboratory of Nonlinear Mechanics,
Institute of Mechanics,
Chinese Academy of Sciences,
Beijing 100190, China;
School of Engineering Science,
University of Chinese Academy of Sciences,
Beijing 100049, China
e-mail: liqinlan@imech.ac.cn

Shuang Li
State Key Laboratory of Nonlinear Mechanics,
Institute of Mechanics,
Chinese Academy of Sciences,
Beijing 100190, China;
School of Engineering Science,
University of Chinese Academy of Sciences,
Beijing 100049, China
e-mail: shuangyangyang123@163.com

Lianqiao Zhou
State Key Laboratory of Nonlinear Mechanics,
Institute of Mechanics,
Chinese Academy of Sciences,
Beijing 100190, China;
School of Engineering Science,
University of Chinese Academy of Sciences,
Beijing 100049, China
e-mail: zhoulianqiao21@mails.ucas.ac.cn

Xinfang Cao
State Key Laboratory of Nonlinear Mechanics,
Institute of Mechanics,
Chinese Academy of Sciences,
Beijing 100190, China;
School of Engineering Science,
University of Chinese Academy of Sciences,
Beijing 100049, China
e-mail: caoxinfang21@mails.ucas.ac.cn

Yuqun Lan
State Key Laboratory of Nonlinear Mechanics,
Institute of Mechanics,
Chinese Academy of Sciences,
Beijing 100190, China;
School of Engineering Science,
University of Chinese Academy of Sciences,
Beijing 100049, China
e-mail: lanyuqun@imech.ac.cn

Xinkai Xu
State Key Laboratory of Nonlinear Mechanics,
Institute of Mechanics,
Chinese Academy of Sciences,
Beijing 100190, China;
School of Engineering Science,
University of Chinese Academy of Sciences,
Beijing 100049, China
e-mail: xuxinkai@imech.ac.cn

Optimal Design Towards High Performance of Sandwich Flexible Piezoelectric Energy Harvesters

The flexible piezoelectric energy harvester (FPEH), as an effective strategy for long-term power supply of implantable and wearable electronics, requires high areal output energy density, low mechanical stiffness, and high energy efficiency, simultaneously. The widely adopted sandwich FPEH, consisting of one relatively hard substrate sandwiched between two piezoelectric films, can provide a high areal output energy density, but also high mechanical stiffness and low energy efficiency due to its energy-wasting deformation of the hard substrate. Here, we propose a novel optimal soft-substrate sandwich FPEH with designs of sufficient length and optimized Young's modulus of the substrate, which is much smaller than that of the piezoelectric film. A sandwich beam model considering both the bending and shearing of the soft substrate and the one-way coupling of the piezoelectric effect was adopted for the theoretical analysis and optimal design. The optimal soft-substrate sandwich FPEH exhibits greatly improved overall performance with a 33% increase in areal output energy density, a 51% reduction in mechanical stiffness, and a 177% increase in energy efficiency, simultaneously. Systematic theoretical analysis is performed to illustrate the mechanism and guide the optimal design. The novel optimal soft-substrate sandwich FPEH is then applied to harvesting energy from various living subjects. This optimal design can be extended to other types of mechanical energy harvesters with a similar laminated structure. [DOI: 10.1115/1.4056818]

Keywords: piezoelectric energy harvesting, piezoelectric analytic model, wearable electronic, implantable electronic, sandwich structure, structural optimization, elasticity, structures

YongAn Huang

State Key Laboratory of Digital Manufacturing
Equipment and Technology,
Flexible Electronics Research Center,
Huazhong University of Science and Technology,
Wuhan 430074, China
e-mail: yahuang@hust.edu.cn

Yuli Chen

Institute of Solid Mechanics,
Beihang University,
Beijing 100191, China
e-mail: yulichen@buaa.edu.cn

Yong Zhao

Key Laboratory of Bioinspired Smart Interfacial
Science and Technology of Ministry of Education,
School of Chemistry,
Beihang University,
Beijing 100191, China
e-mail: zhaoyong@buaa.edu.cn

Chengjun Huang

R&D Center of Healthcare Electronics,
Institute of Microelectronics,
Chinese Academy of Sciences,
Beijing 100029, China
e-mail: huangchengjun@ime.ac.cn

Yanpeng Wei

Key Laboratory for Mechanics in Fluid Solid
Coupling Systems,
Institute of Mechanics,
Chinese Academy of Sciences,
Beijing 100190, China
e-mail: weiyanpeng@imech.ac.cn

Ya Yang

CAS Center for Excellence in Nanoscience,
Beijing Key Laboratory of Micro-Nano, Energy
and Sensor,
Beijing Institute of Nanoenergy and Nanosystems,
Chinese Academy of Sciences,
Beijing 101400, China
e-mail: yayang@binn.cas.cn

Yewang Su[1]

State Key Laboratory of Nonlinear Mechanics,
Institute of Mechanics,
Chinese Academy of Sciences,
Beijing 100190, China;
School of Engineering Science,
University of Chinese Academy of Sciences,
Beijing 100049, China
e-mail: yewangsu@imech.ac.cn

1 Introduction

In recent years, wireless and low-power electronics have been widely developed for implantation in human bodies to monitor physiological parameters and intervene in diseases [1,2], and installation on animals like fish and birds for sensing and tracking [3,4] (Fig. 1(a)[2]). These electronics require not only a lightweight but also an adequate long-term energy supply, which avoids additional replacement surgeries for implantable electronics [5] and ensures a long life in nature for the electronics applied to animals [6]. The flexible piezoelectric energy harvester (FPEH) is a promising solution for these requirements [7–20], as it can harvest electrical energy from the motions of various living subjects [21] (Fig. 1(a)). For practical purposes, the FPEH requires the following mechanical and electric performances simultaneously. (1) **High areal output energy density:** the deformable area of various living subjects is very limited in practice; (2) **low mechanical stiffness:** the FPEH should be flexible enough not to impede the motion of the living subject; (3) **high energy efficiency**: the motions of living subjects can only provide limited mechanical energy.

---

[2]Figure 1(a) is reproduced with permission from www.istockphoto.com
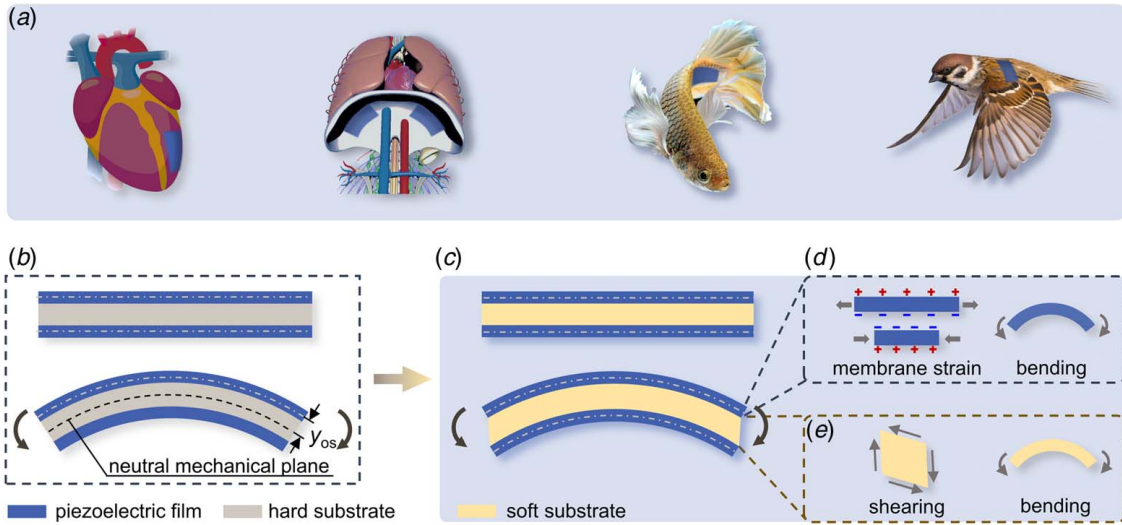
Fig. 1 Illustration of the FPEH: (*a*) electronics and FPEHs applied to various living subjects, including the heart, diaphragm, swimming fish, and flying birds, (*b*) the conventional hard-substrate sandwich FPEH, (*c*) the soft-substrate sandwich FPEH. The bending of the soft-substrate sandwich FPEH results in (*d*) the membrane strain and bending for the piezoelectric film, and (e) the shearing and bending for the soft substrate.

Sandwich FPEHs [22,23] are widely adopted and usually formed by laminating two piezoelectric films on either side of a relatively hard substrate (Fig. 1(*b*)). Structural design is crucial for the FPEH with the sandwich and other laminated structures to meet the above performance requirements, which have been reported in many previous works. For instance, Jung et al. [22] developed a powerful curved sandwich FPEH, where the hard and thick substrate enables a higher output voltage. Chen et al. [8] investigated the effect of Young's moduli of a soft piezoelectric film and relatively hard substrate on the output voltage. The optimal Young's modulus ratio was then determined to maximize the energy output. These works considered only the condition of hard substrate and paid no attention to their negative effects on mechanical stiffness and energy efficiency. Petritz et al. [24] analyzed the effect of the thickness and Young's modulus of the substrate on energy efficiency and concluded that a thick and hard substrate can greatly reduce energy efficiency. These works revealed that the hard substrate can provide sufficient membrane strain of the piezoelectric film and thus a high areal output energy density when bending the FPEH, but it also results in high mechanical stiffness and low energy efficiency due to its energy-wasting deformation. On the other hand, the soft substrate, which is favorable for a flexible design [25], is considered to be unsuitable for the sandwich FPEH, because it may split the neutral mechanical plane (NMP), reduce the membrane strain of the piezoelectric film, and thus lead to a reduced areal output energy density [26]. There are seldom reports on the simultaneous achievement of high areal output energy density, low mechanical stiffness, and high energy efficiency by the structural design of the sandwich FPEH.

In recent years, the soft-substrate sandwich structure, which has been widely adopted in civil engineering and other fields [27], has attracted much attention in the field of flexible electronics [26,28]. Many works have systematically analyzed its mechanical behavior [29,30] and concluded that when the substrate is sufficiently soft, it undergoes mainly shear deformation and the bending strain can be neglected. This results in the split of NMP and the significantly reduced membrane strain of hard films laminated on it [31]. However, our recent works [32] found that soft substrate with sufficient length hardly caused the split of NMP for the sandwich structure. This implies the possibility of adopting a long and soft substrate for the sandwich FPEH to obtain a high output energy density, low mechanical stiffness, and thus high energy efficiency, simultaneously.

In this study, a novel optimal soft-substrate sandwich FPEH is proposed by the theoretical analysis and validated experimentally.

It is designed to have sufficient length and optimized substrate Young's modulus, which is much smaller than that of the piezoelectric film, and has a highly improved overall performance compared to the hard-substrate sandwich FPEH. In the following sections, a systematic theoretical analysis of the influence of various parameters including the length, Young's modulus, and thickness of the substrate on the mechanical and piezoelectric performance of the sandwich FPEH are conducted first. We used a sandwich beam model with plane-strain assumption and soft substrate considering both bending and shearing deformations. Governing equations and boundary conditions were obtained by the variation of the total elastic energy. For the piezoelectric analysis, we considered the one-way coupling between the mechanical and electrical behavior to obtain concise and sufficiently accurate conclusions. The optimal soft-substrate sandwich FPEH is then designed based on the theoretical results, fabricated, and experimentally characterized. Finally, the optimal soft-substrate sandwich FPEHs are applied to harvest energy from the heart, diaphragm, swimming fish, and flying birds to demonstrate practical scenarios and feasibilities.

2 Results and Discussion

2.1 Analytic Model for the Sandwich FPEH. Figure 2(*a*) illustrates the configuration of the sandwich FPEH, with the length $2L$, width W, and thicknesses h_{sub} and h_p for the substrate and the piezoelectric film, respectively. Young's moduli and Poisson's ratios are E_{sub} and ν_{sub} for the substrate, and E_p and ν_p for the piezoelectric films. Both piezoelectric films are coated with ultrathin electrodes on the surfaces and have the polarization $\boldsymbol{P}$ along the thickness direction. The three-point bending (Fig. 2(*b*)) is adopted to simulate the subjected conditions when the FPEHs harvest energy from the living subject. The coordinate system (x, y, z) is established with the origin located at the center of FPEH. With the displacement w_0 caused by the concentrated force F at $x = 0$, the vertical displacement w and the horizontal in-plane displacements u and $-u$ at the central line of the top and bottom piezoelectric film, according to the symmetricity, are yielded, respectively. The soft substrate with E_{sub} ranging from much smaller to similar to E_p is considered here. To simplify the complex coupling behavior of the piezoelectric films and the substrate, the following assumptions are adopted in the analysis. (1) The electrodes coated on the surface of the piezoelectric films are so thin that are ignored in the analysis; (2) the piezoelectric films are modeled as Euler–Bernoulli beams with the membrane strain
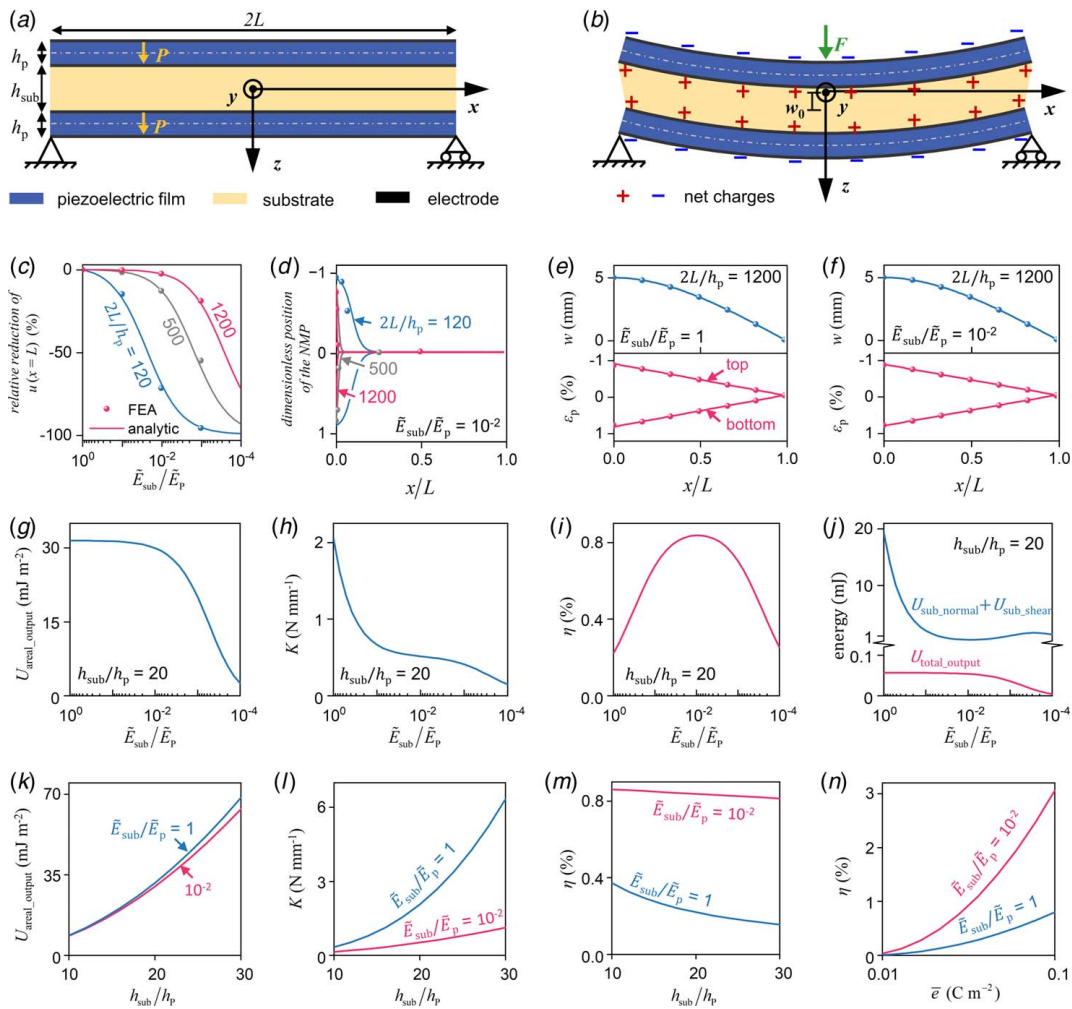
Fig. 2 The universal analytic model for the sandwich FPEH: (*a*) the geometry and boundary conditions for sandwich FPEH, (*b*) the sandwich FPEH is deformed under the three-point bending load, and net charges generate on the electrodes, (*c*) the relative reduction of $u(x=L)$ caused by the decreasing substrate Young's modulus $\tilde{E}_{sub}/\tilde{E}_P$ when the length $2L/h_p$ = 120, 500, and 1200, (*d*) dimensionless position of the NMP along the length of the sandwich FPEH with the lengths $2L/h_p$ = 120, 500, and 1200. The distribution of the vertical displacement w and membrane strain ε_p along the length of the FPEH with $2L/h_p$ = 1200 when, (*e*) $\tilde{E}_{sub}/\tilde{E}_P$ = 1 and (*f*) 10^{-2}. When h_{sub}/h_P = 20, the influence of dimensionless Young's modulus $\tilde{E}_{sub}/\tilde{E}_P$ ranges from 1 to 10^{-4} on the (*f*) theoretical force and output voltage, (*g*) areal output energy density, (*h*) mechanical stiffness, (*i*) energy efficiency, as well as (*j*) elastic energy of the substrate and total output energy. When $\tilde{E}_{sub}/\tilde{E}_P$ = 1 and 10^{-2}, the influence of the dimensionless thickness h_{sub}/h_P ranging from 10 to 30 on the (*k*) areal output energy density, (*l*) mechanical stiffness, (*m*) energy efficiency, and (*n*) equivalent piezoelectric constant.

$$\varepsilon_p = \frac{du}{dx} \tag{1}$$

and $-\varepsilon_p$ for the top and bottom films, respectively, and bending curvature (Fig. 1(*d*))

$$\kappa_p = \frac{d^2 w}{dx^2} \tag{2}$$

(3) the substrate involves not only the bending strain ε_{sub} but also the non-negligible shear strain γ_{sub} [33,34] (Fig. 1(*e*)). The continuity of the interface between the piezoelectric film and the substrate, together with assumptions of the linear and constant distributions along the thickness direction for the bending strain and shear strain respectively, gives

$$\begin{cases} \varepsilon_{sub} = \dfrac{-2\varepsilon_p + \kappa_p h_p}{h_{sub}} z \\ \gamma_{sub} = \dfrac{dw}{dx} + \dfrac{1}{h_{sub}}\left(-2u + h_p \dfrac{dw}{dx}\right) \end{cases} \tag{3}$$

(see Appendix A for more details), and (4) the plane-strain condition is applied to the entire analytic model.

To obtain a concise and accurate enough result and capture the key factors of the structural optimization of the sandwich FPEH, the one-way coupling between the mechanical and electric behaviors that neglects the effect of piezoelectric voltage on the mechanical deformation is adopted. The one-way coupling is applicable because: (1) the total electric output energy is usually much smaller than the total elastic energy in practice and the sandwich FPEH has no additional electric energy input from outside; (2) the deformation of sandwich FPEH is restricted by the living subjects and can be hardly influenced by the piezoelectric voltage. The total elastic energy of the FPEH $U_{elastic}$ consists of the bending and membrane energy of the two piezoelectric films, and the energy yielded by the normal strain and shear strain of the substrate, i.e.,

$$U_{elastic} = U_{p\_bending} + U_{p\_membrane} + U_{sub\_normal} + U_{sub\_shear} \tag{4}$$

Here,

$$
\begin{cases}
U_{\text{p\_bending}} = \frac{1}{6}\tilde{E}_p W h_p^3 \int_0^L \kappa_p^2 \, dx \\[4pt]
U_{\text{p\_membrane}} = 2 W \tilde{E}_p h_p \int_0^L \varepsilon_p^2 \, dx \\[4pt]
U_{\text{sub\_normal}} = W \tilde{E}_{\text{sub}} \int_0^L dx \int_{-h_{\text{sub}}/2}^{h_{\text{sub}}/2} \varepsilon_{\text{sub}}^2 \, dz \\[4pt]
U_{\text{sub\_shear}} = \frac{1}{2}\tilde{E}_{\text{sub}} W h_{\text{sub}}(1-\nu_{\text{sub}}) \int_0^L \gamma_{\text{sub}}^2 \, dx
\end{cases}
\tag{5}
$$

in which $\tilde{E}_p = E_p/(1-\nu_p^2)$ and $\tilde{E}_{\text{sub}} = E_{\text{sub}}/(1-\nu_{\text{sub}}^2)$ are the plane-strain Young's moduli of the piezoelectric film and substrate, respectively. Substituting Eqs. (1)–(3), and (5) into Eq. (4), we have the total elastic energy

$$
U_{\text{elastic}} = \frac{1}{6}\tilde{E}_p W h_p^3 \int_0^L \left(\frac{d^2 w}{dx^2}\right)^2 dx + 2 W \tilde{E}_p h_p \int_0^L \left(\frac{du}{dx}\right)^2 dx
$$
$$
+ W \tilde{E}_{\text{sub}} \int_0^L dx \int_{-h_{\text{sub}}/2}^{h_{\text{sub}}/2} \left(\frac{-2\varepsilon_p + \kappa_p h_p}{h_{\text{sub}}}\right)^2 z^2 \, dz
$$
$$
+ \frac{1}{2}\tilde{E}_{\text{sub}} W h_{\text{sub}}(1-\nu_{\text{sub}}) \int_0^L \left(1 + \frac{-2u + h_p}{h_{\text{sub}}}\right)^2 \left(\frac{dw}{dx}\right)^2 dx
\tag{6}
$$

The variation of Eq. (6), with the condition of the symmetry along the z-axis, gives the governing equations for u and w of the sandwich FPEH [34]

$$
\begin{cases}
\dfrac{d^4 w}{dx^4} - a\dfrac{d^2 w}{dx^2} - b\dfrac{du}{dx} + e\dfrac{d^3 u}{dx^3} = 0 \\[8pt]
\dfrac{d^2 u}{dx^2} - \dfrac{ac}{b}\dfrac{dw}{dx} - cu + \dfrac{ace}{b^2}\dfrac{dw^3}{dx^3} = 0
\end{cases}
\tag{7}
$$

and the boundary conditions

$$
\begin{cases}
u(0) = 0, \; w(0) = w_0, \; \left.\dfrac{dw}{dx}\right|_{x=0} = 0 \\[8pt]
\left.\dfrac{du}{dx}\right|_{x=L} = 0, \; w(L) = 0, \; \left.\dfrac{d^2 w}{dx^2}\right|_{x=L} = 0
\end{cases}
\tag{8}
$$

where

$$
a = \frac{6(1-\nu_{\text{sub}})(1+h_p/h_{\text{sub}})^2}{h_p^2[2\tilde{E}_p h_p/(\tilde{E}_{\text{sub}}h_{\text{sub}})+1]}, \quad b = \frac{-12(1-\nu_{\text{sub}})(1+h_p/h_{\text{sub}})}{h_{\text{sub}}h_p^2[2\tilde{E}_p h_p/(\tilde{E}_{\text{sub}}h_{\text{sub}})+1]}
$$
$$
c = \frac{6(1-\nu_{\text{sub}})}{h_{\text{sub}}^2[6\tilde{E}_p h_p/(\tilde{E}_{\text{sub}}h_{\text{sub}})+1]}, \quad e = -\frac{2}{h_p[2\tilde{E}_p h_p/(\tilde{E}_{\text{sub}}h_{\text{sub}})+1]}
\tag{9}
$$

Solving the governing equations with the boundary conditions, we have the displacements

$$
\begin{cases}
w = [H_{w0} + H_{w1}x + H_{w2}x^2 + H_{w3}x^3 + H_{w4}\sinh(sx-sL)]w_0 \\[4pt]
u = [H_{u0} + H_{u1}x + H_{u2}x^2 + H_{u3}\cosh(sx-sL)]w_0
\end{cases}
\tag{10}
$$

for the right half of the sandwich FPEH ($0 \leq x \leq L$), where s and H with subscript are the constants related to the sizes and mechanical parameters of the sandwich FPEH and shown in Appendix B. Furthermore, the distribution of the membrane strain of the piezoelectric films ε_p, the curvature of the piezoelectric films κ_p, as well as the normal and shear strain of the substrate ε_{sub} and γ_{sub} along the length of the FPEH are obtained,

$$
\begin{cases}
\varepsilon_p = [H_{u1} + 2H_{u2}x + sH_{u3}\sinh(sx-sL)]w_0 \\[4pt]
\kappa_p = [2H_{w2} + 6H_{w3}x + s^2 H_{w4}\sinh(sx-sL)]w_0 \\[4pt]
\varepsilon_{\text{sub}} = [(2h_p H_{w2} - 2H_{u1}) + (6h_p H_{w3} - 4H_{u2})x + (h_p s^2 H_{w4} - 2sH_{u3})\sinh(sx-sL)]z\dfrac{w_0}{h_{\text{sub}}} \\[4pt]
\gamma_{\text{sub}} = \left\{ \begin{aligned} &\left[\left(1+\frac{h_p}{h_{\text{sub}}}\right)H_{w1} - \frac{2H_{u0}}{h_{\text{sub}}}\right] + \left[2H_{w2}\left(1+\frac{h_p}{h_{\text{sub}}}\right) - \frac{2H_{u1}}{h_{\text{sub}}}\right]x \\ &+ \left[3H_{w3}\left(1+\frac{h_p}{h_{\text{sub}}}\right) - \frac{2H_{u2}}{h_{\text{sub}}}\right]x^2 + \left[sH_{w4}\left(1+\frac{h_p}{h_{\text{sub}}}\right) - \frac{2H_{u3}}{h_{\text{sub}}}\right]\cosh(sx-sL) \end{aligned} \right\} w_0
\end{cases}
\tag{11}
$$

The dimensionless location of the NMP of the top and bottom piezoelectric film can be obtained as

$$
\bar{z}_{\text{top}} = -\bar{z}_{\text{bottom}} = \left(\frac{\varepsilon_p}{\kappa_p} - \frac{h_p + h_{\text{sub}}}{2}\right) \bigg/ \left(\frac{2h_p + h_{\text{sub}}}{2}\right)
\tag{12}
$$

Substituting Eqs. (11) and (5) into Eq. (4), we then obtain the total elastic energy

$$
U_{\text{elastic}} = \left\{ \begin{aligned}
&\frac{\tilde{E}_p W h_p^3}{6}\int_0^L [2H_{w2} + 6H_{w3}x + s^2 H_{w4}\sinh(sx-sL)]^2 \, dx \\[4pt]
&+ 2W\tilde{E}_p h_p \int_0^L [H_{u1} + 2H_{u2}x + sH_{u3}\sinh(sx-sL)]^2 \, dx \\[4pt]
&+ W\tilde{E}_{\text{sub}}\int_0^L dx \int_{-h_{\text{sub}}/2}^{h_{\text{sub}}/2} \left[\begin{aligned}&(2h_p H_{w2} - 2H_{u1}) + (6h_p H_{w3} - 4H_{u2})x \\ &+ (h_p s^2 H_{w4} - 2sH_{u3})\sinh(sx-sL)\end{aligned}\right]^2 \left(\frac{z}{h_{\text{sub}}}\right)^2 dx \\[4pt]
&+ \frac{1}{2}\tilde{E}_{\text{sub}} W h_{\text{sub}}(1-\nu_{\text{sub}}) \int_0^L \left\{\begin{aligned}&\left[\left(1+\frac{h_p}{h_{\text{sub}}}\right)H_{w1} - \frac{2H_{u0}}{h_{\text{sub}}}\right] \\ &+ \left[2H_{w2}\left(1+\frac{h_p}{h_{\text{sub}}}\right) - \frac{2H_{u1}}{h_{\text{sub}}}\right]x \\ &+ \left[3H_{w3}\left(1+\frac{h_p}{h_{\text{sub}}}\right) - \frac{2H_{u2}}{h_{\text{sub}}}\right]x^2 \\ &+ \left[sH_{w4}\left(1+\frac{h_p}{h_{\text{sub}}}\right) - \frac{2H_{u3}}{h_{\text{sub}}}\right]\cosh(sx-sL)\end{aligned}\right\}^2 dx
\end{aligned} \right\} w_0^2
\tag{13}
$$

and the theoretical force $F = 2U_{\text{elastic}}/w_0$. With the $D - \varepsilon$ type piezoelectric constitutive equation

$$D_3 = \bar{e}\varepsilon_p - \frac{\bar{k}V}{h_p} \qquad (14)$$

the open-circuit condition $4W\int_0^L D_3 \mathrm{d}x = 0$, and the total capacitance $C_p = 4\bar{k}WL/h_p$, the output voltage of the two piezoelectric films connected in parallel is yielded as

$$V = \frac{\bar{e}}{\bar{k}}\frac{h_p}{L}(H_{u0} + H_{u1}L + H_{u2}L^2)w_0 \qquad (15)$$

Here, D_3, $\bar{e} = (d_{31} + \nu_p d_{32})\tilde{E}_p$, and $\bar{k} = k_{33} - \tilde{E}_p(d_{31} + \nu_p d_{32})^2 - E_p d_{32}^2$ are the electric displacement, the equivalent piezoelectric constant, and the equivalent permittivity; k_{33}, d_{31}, and d_{32} are the permittivity and the piezoelectric constants, respectively (see Appendix C for more details). Furthermore, total electric energy output can be calculated by $U_{\text{total\_output}} = C_p V^2/2$. Key parameters for the overall performance of the sandwich FPEH, including the areal output energy density $U_{\text{areal\_output}}$ (the total electric energy output divided by the area of the sandwich FPEH), the mechanical stiffness K (the ratio between the force F and the vertical displacement w_0), and the energy efficiency η (the ratio between the total electric output energy and the work of force $Fw_0/2$) can be expressed as

$$U_{\text{areal\_output}} = C_p V^2/(4LW), \quad K = F/w_0, \quad \text{and}\ \eta = C_p V^2/(Fw_0) \qquad (16)$$

respectively.

2.2 Theoretical Analysis for the Sandwich FPEH.

A group of typical mechanical and piezoelectric parameters $h_p = 50\ \mu m$, $h_{\text{sub}} = 1\ \text{mm}$ ($h_{\text{sub}}/h_p = 20$), $W = 3\ \text{cm}$, $E_p = 2.45\ \text{GPa}$, $\nu_p = \nu_{\text{sub}} = 0.35$, $d_{31} = -17\ \text{pC N}^{-1}$, $d_{32} = -5\ \text{pC N}^{-1}$, $k_{33} = 84.08\ \text{pF m}^{-1}$ with different lengths $2L$ and Young's moduli of the substrate E_{sub} are considered here. The influences of the length on the mechanical behavior of the sandwich FPEH with a soft substrate $\tilde{E}_{\text{sub}}/\tilde{E}_p < 1$ are studied first. To present the results concisely, we consider the in-plane horizontal displacement at the end of the piezoelectric film $u(x = L) = (H_{u0} + H_{u1}L + H_{u2}L^2)w_0$, which is the integral of the membrane strain from $x = 0$ to L and is directly related to the output voltage (Eq. (15)). Figure 2(c) shows its relative reduction produced by the decreasing of substrate Young's modulus $\tilde{E}_{\text{sub}}$, compared to the condition of a conventional hard substrate ($\tilde{E}_{\text{sub}}/\tilde{E}_p = 1$) with different dimensionless lengths $2L/h_p = 120$, 500, and 1200, respectively. It can be seen that for the short sandwich FPEH with $2L/h_p = 120$, the $u(x = L)$ decreases rapidly with the decreasing substrate Young's modulus $\tilde{E}_{\text{sub}}$, but remains almost unchanged until $\tilde{E}_{\text{sub}}/\tilde{E}_p$ is below 10^{-2} for the long sandwich FPEH with $2L/h_p = 1200$. Our previous findings suggest that this may be caused by the splitting of the NMP [34]. According to the plane section assumption of the Euler–Bernoulli beam theory, the piezoelectric films and substrate of the hard-substrate sandwich FPEH share one NMP, which is located in the central plane of the entire FPEH due to symmetry. Deviation from the NMP brings a large membrane strain of the piezoelectric film. As the substrate softens, the top and bottom piezoelectric film tend to bend independently, with their NMPs split and moving toward them, respectively. This reduces the distance between the NMP and the central plane of the piezoelectric film, resulting in reduced membrane strain. We calculate the distribution of the dimensionless position of the NMP along the length x/L for the soft-substrate sandwich FPEH with $\tilde{E}_{\text{sub}}/\tilde{E}_p = 10^{-2}$ and different lengths, as shown in Fig. 2(d). The NMP of the sandwich FPEH with $2L/h_p = 120$ splits in two and deflects very close to the top and bottom piezoelectric films. In contrast, the NMP of the longer sandwich FPEH with $2L/h_p = 1200$ only split in a very small

section near the center of the FPEH. This ensures that the distributions of both vertical displacement w and membrane strain ε_p are almost the same at $\tilde{E}_{\text{sub}}/\tilde{E}_p = 1$ and 10^{-2}, as shown in Figs. 2(e) and 2(f). The above results are validated by the finite element analysis (FEA), whose details are shown in Appendix D.

The influence of $\tilde{E}_{\text{sub}}$ on the areal output energy density $U_{\text{areal\_output}}$, the mechanical stiffness K, and the energy efficiency η of the long sandwich FPEH with $2L/h_p = 1200$ are studied further. The results for $\tilde{E}_{\text{sub}}/\tilde{E}_p$ ranging from 1 to 10^{-4}, $h_{\text{sub}}/h_p = 20$, and $w_0 = 5\ \text{mm}$ are shown in Figs. 2(g)–2(i). When $\tilde{E}_{\text{sub}}/\tilde{E}_p$ reduces from 1 to 10^{-2}, the areal output energy density $U_{\text{areal\_output}}$ only dips by 4.9% (from 31.52 mJ m^{-2} to 29.98 mJ m^{-2}), while mechanical stiffness K slashes by 75% (from 2.06 N mm^{-1} to 0.52 N mm^{-1}), and the energy efficiency η grows by 282% (from 0.22% to the maximum energy efficiency $\eta_{\text{max}} = 0.84\%$). However, when $\tilde{E}_{\text{sub}}/\tilde{E}_p$ drops below 10^{-2}, both the areal output energy density $U_{\text{areal\_output}}$ and energy efficiency η decay significantly, resulting in a great reduction in the performance of the FPEH. The change of the substrate elastic energy $U_{\text{sub\_normal}} + U_{\text{sub\_shear}}$ and the total electric energy output $U_{\text{total\_output}}$ with $\tilde{E}_{\text{sub}}/\tilde{E}_p$ are shown in Figs. 2(j) and S1 available in the Supplemental Materials on the ASME Digital Collection. When $\tilde{E}_{\text{sub}}/\tilde{E}_p$ drops from 1 to 10^{-2}, the rapidly decreasing $U_{\text{sub\_normal}} + U_{\text{sub\_shear}}$ causes a reduction of the force F. The $U_{\text{sub\_normal}} > U_{\text{sub\_shear}}$ indicates that bending dominates the deformation of the substrate; the shear strain, which can induce a reduction of the membrane strain of the piezoelectric film, is quite small, resulting in an almost unchanged U_{electric}. However, the $U_{\text{sub\_shear}}$ becomes greater than $U_{\text{sub\_normal}}$ when $10^{-2} > \tilde{E}_{\text{sub}}/\tilde{E}_p > 10^{-4}$. This indicates that the substrate is dominated by the shear deformation and acted as a "shear lag," resulting in the reduction of $U_{\text{total\_output}}$ and η. Above results reveal the existence of the optimal $\tilde{E}_{\text{sub}}$ for a long enough soft-substrate sandwich FPEH. It can be obtained at the transition ($\tilde{E}_{\text{sub}}/\tilde{E}_p = 10^{-2}$ for the length of $2L/h_p = 1200$) between the bending- and shear-dominated deformation, reduces the mechanical stiffness greatly, and maximizes the energy efficiency η, with a bare reduction of the areal output energy density.

Furthermore, for the conventional hard-substrate ($\tilde{E}_{\text{sub}}/\tilde{E}_p = 1$) and the optimal soft-substrate ($\tilde{E}_{\text{sub}}/\tilde{E}_p = 10^{-2}$) sandwich FPEHs with $2L/h_p = 1200$, the changes in the areal output energy density $U_{\text{areal\_output}}$, the mechanical stiffness K, and energy efficiency η as the dimensionless thickness h_{sub}/h_p ranging from 10 to 30 are studied as well and shown in Figs. 2(k)–2(m). For the hard-substrate sandwich FPEH with $\tilde{E}_{\text{sub}}/\tilde{E}_p = 1$, the mechanical stiffness K multiplies much faster than the $U_{\text{areal\_output}}$ (18.9 and 7.9 times, respectively) with the increasing h_{sub}/h_p (from 10 to 30), resulting in a significant reduction in the energy efficiency η (by 58%). This suggests that the increase of h_{sub} is not an efficient way toward the higher areal output energy density $U_{\text{areal\_output}}$ for the conventional hard-substrate sandwich FPEH. On the other hand, for the optimal soft-substrate sandwich FPEH with $\tilde{E}_{\text{sub}}/\tilde{E}_p = 10^{-2}$, $U_{\text{areal\_output}}$ has a similar increasing trend to that of the hard-substrate sandwich FPEH; but K is keeping a low level, making the energy efficiency η more insensitive to h_{sub} (only decreased by 5.5% from $h_{\text{sub}}/h_p = 10$ to 30). This means that adopting a thicker optimal $\tilde{E}_{\text{sub}}$ can yield a higher areal output energy density, lower mechanical stiffness, and higher energy efficiency, simultaneously. In addition, taking the effective piezoelectric constant $\bar{e}$ as an example, the improvement of the piezoelectric properties results in a greater improvement of the energy efficiency η of the optimal soft-substrate sandwich FPEH. (Figure 2(n)) This implies that when developing high-performance piezoelectric materials [10,12,18,19], adopting the optimal soft-substrate sandwich structure can utilize the material properties better and enlarge its positive effect on the overall performance of the FPEH significantly.

2.3 Fabrication and Performance Characterization of the Optimal Soft-Substrate Sandwich FPEH.

A 1.0-mm-thick optimal soft-substrate sandwich FPEH (Figs. 3(a)
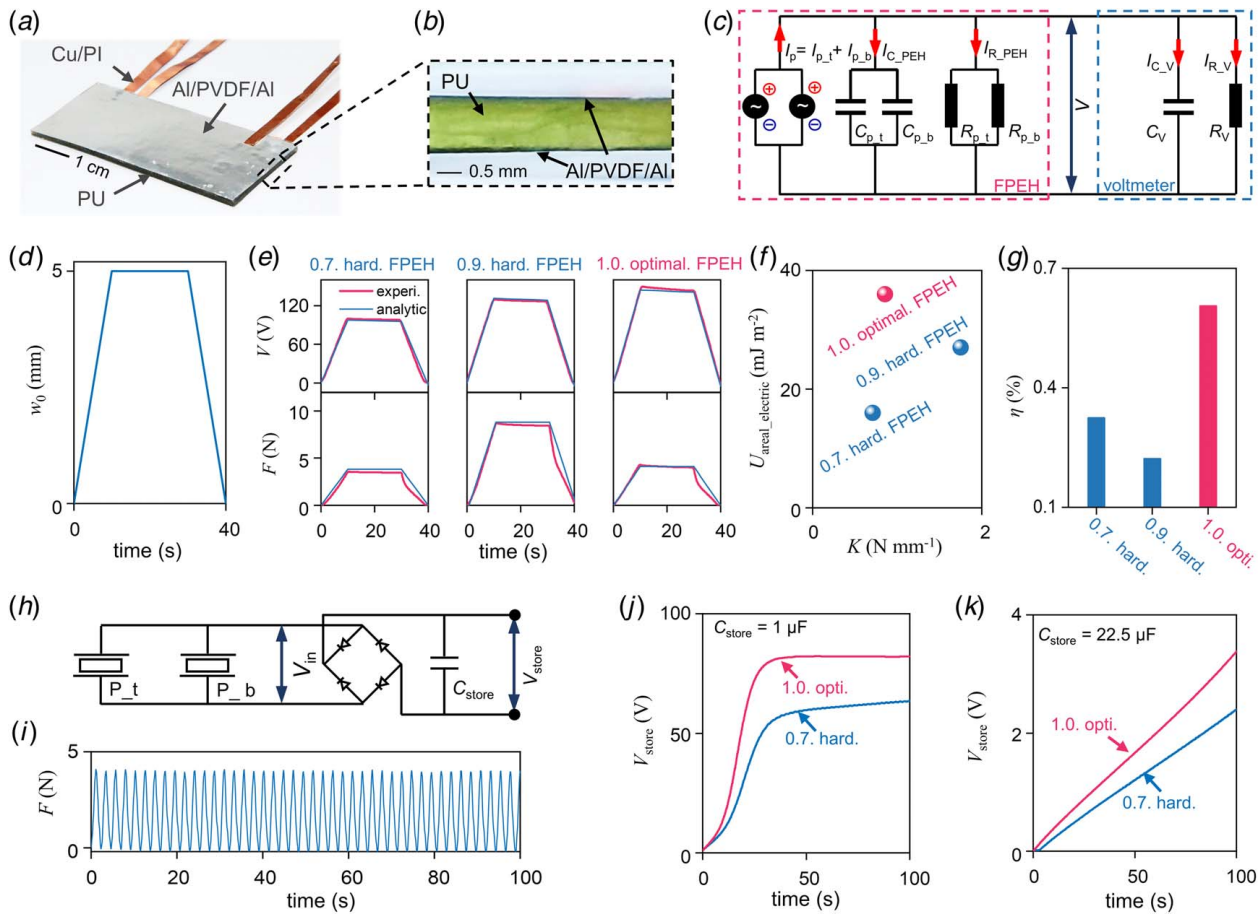
Fig. 3 Experimental characterization of the sandwich FPEHs. The photograph of (a) the fabricated 1.0-mm-thick optimal soft-substrate sandwich FPEH, (b) the enlarged side view, (c) schematic illustration of the measurement circuit including the two current sources, two capacitances, and two resistances of the sandwich FPEH, as well as the capacitance and resistance of the voltmeter, (d) the displacement load on the sandwich FPEH, (e) the measured and theoretical force and voltage of the 0.7-mm-thick hard-substrate, 0.9-mm-thick hard-substrate, and 1.0-mm-thick optimal soft-substrate sandwich FPEH, (f) the areal output energy density, mechanical stiffness, (g) the energy efficiency of the three sandwich FPEHs obtained from the experimental results, (h) the circuit model of the sandwich FPEH charging a capacitor through a rectifier bridge, (i) the corresponding force of the 1.0-mm-thick optimal soft-substrate for the periodic loading. The voltage results V_{store} of the capacitor with (j) $C_{store} = 1\,\mu F$ and (k) 22.5 μF charged by the 0.7-mm-thick hard-substrate and 1.0-mm-thick optimal soft-substrate sandwich FPEH.

and 3(b)) with $2L = 6$ cm, $W = 3$ cm, $h_p = 55\,\mu m$, $h_{sub} = 1.018$ mm, and the optimal $\tilde{E}_{sub}/\tilde{E}_p = 0.011$ ($E_p = 2.45$ GPa, $\nu_p = 0.35$, $E_{sub} = 24.91$ MPa, and $\nu_{sub} = 0.4$) was designed and fabricated according to the theoretical results. The piezoelectric films were made from commercial polyvinylidene fluoride (PVDF) film with thickness-negligible aluminum coatings as electrodes on the surface. The Cu/Polyimide (Cu/PI) narrow ribbons were pasted on the electrodes with a conductive silver adhesive to connect the two piezoelectric films in parallel and to the external circuit. After that, the two piezoelectric films were pasted on both sides of an optimal soft substrate made from polyurethane (PU) by the hard PU adhesive with the thickness of the bonding layer $h_{bond} = 20\,\mu m$. d_{31}, d_{32}, and k_{33} of the PVDF films are the same as in the last section, with the resistivity $\rho_p = 1 \times 10^{13}$ Ωm. As a comparison, two conventional hard-substrate sandwich FPEHs with $h_{sub} = 0.671$ mm (0.7-mm-thick hard-substrate sandwich FPEH) and $h_{sub} = 0.921$ mm (0.9-mm-thick hard-substrate sandwich FPEH) were prepared with the polyethylene terephthalate (PET) film as the hard substrate ($\tilde{E}_{sub}/\tilde{E}_p = 1.05$). A mechanical test machine was used to perform the three-point bending test with displacement loading $w_{0\_max} = 5$ mm at the rate 0.5 mm s^{-1}, as shown in Fig. 3(d). The output voltage V, measured by a voltmeter (Keithley 6517B, with inner resistance $R_V = 200$ TΩ and capacitance $C_V = 360$ pF), and the force F of the three sandwich FPEHs are shown in Fig. 3(d).

Details of the fabrication and experiments process were shown in Appendix E. The maximum output voltages and forces obtained when $w_0 = w_{0\_max}$ were ($V_{max} = 99.61$ V, $F_{max} = 3.55$ N) for the 0.7-mm-thick hard-substrate sandwich FPEH, ($V_{max} = 129.54$ V, $F_{max} = 8.75$ N) for the 0.9-mm-thick hard-substrate sandwich FPEH, and ($V_{max} = 149.53$ V, $F_{max} = 4.28$ N) for the 1.0-mm-thick optimal soft-substrate sandwich FPEH, respectively.

In practice, the measured voltages depended on not only the capacitance and resistance of the FPEH but also the capacitance and resistance of the voltmeter. As shown in Fig. 3(c) [33], the sandwich FPEH, whose top and bottom piezoelectric films are connected in parallel, can be regarded as the parallel connection of two current sources, two capacitances, and two resistances

$$\begin{cases} I_p = I_{p\_t} + I_{p\_b} = 4W\bar{e}(H_{u0} + H_{u1}L + H_{u2}L^2)\dfrac{dw_0}{dt} \\ C_p = C_{p\_t} + C_{p\_t} = \dfrac{4\bar{k}WL}{h_p} \\ R_p = \dfrac{1}{1/R_{p\_t} + 1/R_{p\_b}} = \dfrac{\rho_p h_p}{4LW} \end{cases} \quad (17)$$

where p_t and p_b indicate the top and bottom piezoelectric film, respectively. The measurement circuit can be regarded as the

parallel connection of the sandwich FPEH, and the capacitance C_V and resistance R_V of the voltmeter. Thus, we have the total capacitance and resistance of the circuit

$$\begin{cases} C = \dfrac{4\bar{k}WL}{h_p} + C_V \\ R = \dfrac{1}{4LW/(\rho_p h_p) + 1/R_V} \end{cases} \qquad (18)$$

According to Ohm's law and the I–V relationship of the capacitance, the current flow into the capacitance of the FPEH $I_{C\_PEH} = (4\bar{k}WL/h_p)dV/dt$ and the voltmeter $I_{C\_V} = C_V dV/dt$, and through the resistance of the FPEH $I_{R\_PEH} = V/[\rho_p h_p/(4LW)]$ and the voltmeter $I_{R\_V} = V/R_V$ can be obtained. With the conservation of current

$$I_p = I_{C\_PEH} + I_{R\_PEH} + I_{C\_V} + I_{R\_V} \qquad (19)$$

the differential equation of the output voltage

$$C\frac{dV}{dt} + \frac{V}{R} = 4W\bar{e}(H_{u0} + H_{u1}L + H_{u2}L^2)\frac{dw_0}{dt} \qquad (20)$$

can be obtained. With the initial condition $V|_{t=0} = 0$, the output voltage of the sandwich FPEH is yielded as

$$V = \frac{4W\bar{e}(H_{u0} + H_{u1}L + H_{u2}L^2)}{C}w_0$$
$$- \frac{4W\bar{e}(H_{u0} + H_{u1}L + H_{u2}L^2)}{RC^2}e^{-\frac{t}{RC}}\int_0^t w_0 e^{\frac{t}{RC}}dt \qquad (21)$$

Details of the derivation are shown in Appendix F. In the theoretical model, the thin bonding layers of the hard-substrate sandwich FPEHs are ignored, while the bonding layers of the 1.0-mm-thick optimal soft-substrate sandwich FPEH are thick and much harder than the soft substrate, and cannot be ignored (Fig. S3 available in the Supplemental Materials on the ASME Digital Collection). Assuming that the bonding layer has the same plane-strain Young's modulus as the piezoelectric film, the theoretical results for 1.0-mm-thick optimal soft-substrate sandwich FPEH are modified by replacing h_p with $h_p + h_{bond}$ for the mechanical results. Then, Eq. (9) is modified as

$$\begin{cases} a = \dfrac{6(1-\nu_{sub})[1+(h_p+h_{bond})/h_{sub}]^2}{(h_p+h_{bond})^2[2\tilde{E}_p(h_p+h_{bond})/(\tilde{E}_{sub}h_{sub})+1]} \\ b = \dfrac{-12(1-\nu_{sub})[1+(h_p+h_{bond})/h_{sub}]}{h_{sub}(h_p+h_{bond})^2[2\tilde{E}_p(h_p+h_{bond})/(\tilde{E}_{sub}h_{sub})+1]} \\ c = \dfrac{6(1-\nu_{sub})}{h_{sub}^2[6\tilde{E}_p(h_p+h_{bond})/(\tilde{E}_{sub}h_{sub})+1]} \\ e = \dfrac{-2}{(h_p+h_{bond})[2\tilde{E}_p(h_p+h_{bond})/(\tilde{E}_{sub}h_{sub})+1]} \end{cases} \qquad (22)$$

and the coefficients H_{u0}, H_{u1}, and H_{u2} of the output voltage (Eqs. (17)–(21)), are replaced by

$$H_{u0}^m = H_{u0} + \frac{1}{2}h_b H_{w1}, H_{u1}^m = H_{u1} + h_b H_{w2}, \text{ and } H_{u2}^m = H_{u2} + \frac{3}{2}h_b H_{w3} \qquad (23)$$

respectively (see Appendix G for more details). The theoretical output voltage and force of the three sandwich FPEHs were in good agreement with the experiments, as shown in Fig. 3(e).

The experimental results of the areal output energy density $U_{areal\_output} = CV_{max}^2/(4LW)$, the mechanical stiffness $K = F_{max}/w_{0\_max}$, and the energy efficiency $\eta = CV_{max}^2/(F_{max}w_{0\_max})$ at $w_{0\_max} = 5$ mm of all three sandwich FPEHs were shown in Figs. 3(f) and 3(g). Comparing the two hard-substrate sandwich FPEHs, the increased h_{sub} only promoted the U_{areal_output} from 15.97 mJ m^{-2} to 27.01 mJ m^{-2}, by 69%, while escalating the mechanical stiffness K from 0.71 N mm^{-1} to 1.75 N mm^{-1}, by

146%, resulting in a 31% reduction in the energy efficiency η. Furthermore, comparing the 1.0-mm-thick optimal soft-substrate sandwich FPEH with the 0.9-mm-thick hard-substrate sandwich FPEH, the optimal $\tilde{E}_{sub}$ and the increased h_{sub} ramped up the areal output energy density U_{areal_output} by 33% (to 35.99 mJ m^{-2}), slashed the mechanical stiffness K by 51% (to 0.86 N mm^{-1}), and raised the energy efficiency by 177% (from 0.22% to 0.61%), simultaneously. Herein, the greatly increased energy efficiency was still not very outstanding due to the low piezoelectric constant of the commercial piezoelectric material we used. When using higher-performance piezoelectric materials, according to Fig. 2(n), the optimal structure can lead to a greater improvement in the performance of the sandwich FPEH. In practical applications, the sandwich FPEH is usually used to charge an energy storage device like a capacitor and battery, and electronics are powered by the energy storage device. Herein, both the optimal soft-substrate sandwich FPEH and the 0.7-mm-thick hard-substrate, with similar mechanical stiffness, were used to charge capacitors with $C_{store} = 1$ μF and 22.5 μF through a rectifier bridge (Fig. 3(h)) under the same period displacement loading ($w_{0\_max} = 5$ mm at the rate of 5 mm s^{-1}). With a similar force response (Figs. 3(i) and S2 available in the Supplemental Materials), the charging results in Figs. 3(j) and 3(k) showed that the optimal soft-substrate sandwich FPEH had both a higher saturating voltage and a faster-charging speed compared to the 0.7-mm-thick-hard-substrate sandwich FPEH.

2.4 Harvesting Energy From the Motion of Organs and Organisms With the Optimal Soft-Substrate Sandwich FPEH. When harvesting energy from living subjects in practice, a suitable mechanical stiffness is very important for the optimal soft-substrate sandwich FPEH. It can be realized by adjusting the thickness of the substrate h_{sub} without changing the energy efficiency very much. Herein, another 0.6-mm-thick optimal soft-substrate sandwich FPEH ($h_{sub} = 0.636$ mm and $K = 0.24$ N mm^{-1}) was designed and fabricated, together with the 1.0-mm-thick optimal soft-substrate sandwich FPEH mentioned in the last section ($h_{sub} = 1.058$ mm and $K = 0.85$ N mm^{-1}), to harvest energy from the movement of various organs, such as the heart (Fig. 4(a)) and diaphragm (Fig. 4(d)), as well as various organisms, such as the fish (Fig. 4(f)) and birds (Fig. 4(j)).

To demonstrate the ability of the optimal soft-substrate sandwich FPEH to harvest energy from the heartbeat, an artificial soft heart (Fig. 4(a) and S4 available in the Supplemental Materials) was 3D printed by the PolyJet process from a soft material with a hardness of 30A [35]. The artificial soft heart consists of a left ventricle, a right ventricle (RV), and an expansion chamber (EC) between them. The heartbeat was simulated by inflating and deflating the EC periodically by a pressurized air source ($p = 0.2$ kPa) under the control of a pulse signal. The fluid circulated from the central vein, through the RV, and to the pulmonary artery exhibits at this time. (Figure 4(b)) The 0.6-mm-thick optimal soft-substrate sandwich FPEH was pasted on the outer wall of the RV and deformed periodically driven by the heartbeat with a rate of 60 bpm. The periodic output voltage with a peak value of 8.8 V was measured by a 10-MΩ-resistance voltmeter and shown in Fig. 4(c). To demonstrate the ability of the optimal soft-substrate sandwich FPEH to harvest energy from the diaphragm during breathing, an artificial diaphragm was fabricated by attaching a patterned 1-mm-thick PU plate to a human sternum model (Fig. 4(d)). The inhalation and exhalation were simulated by inflating and deflating a balloon using pressurized air ($p = 0.2$ kPa), leading to a periodical deformation of the artificial diaphragm. Two 1.0-mm-thick optimal soft-substrate sandwich FPEHs were symmetrically attached to the diaphragm when breathing at the rate of ~0.5 Hz. Measured by the 10-MΩ-resistance voltmeter, the left and right sandwich FPEH output periodic voltages with peak values of ~55 V and ~45 V, respectively (Fig. 4(e)).
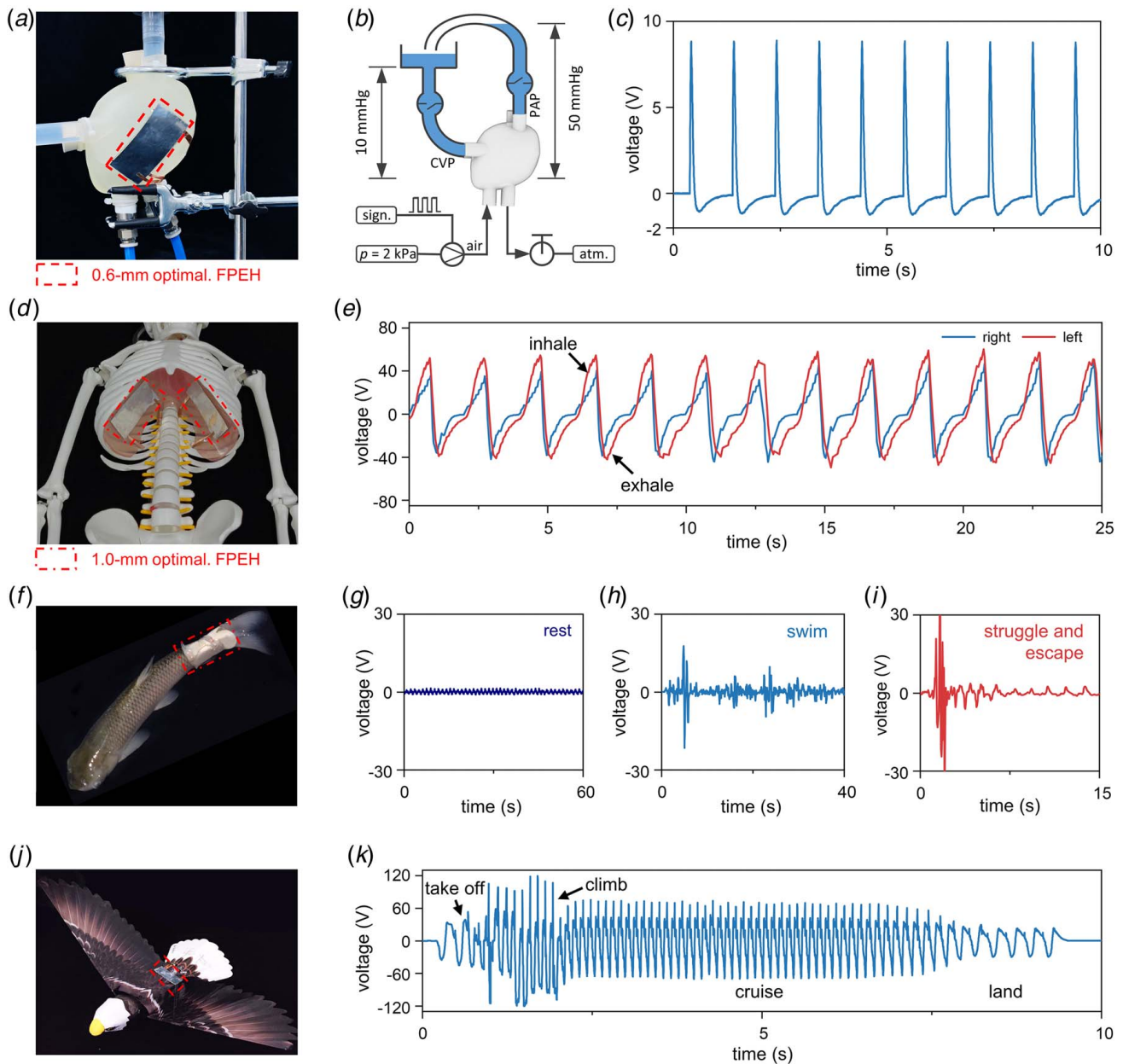
Fig. 4 Applications of the optimal soft-substrate sandwich FPEHs: (a) the photograph of a 0.6-mm-thick optimal soft-substrate sandwich FPEH installed on the artificial heart, (b) the driving systems to simulate the heartbeat, (c) output voltages of the 0.6-mm-thick optimal soft-substrate sandwich FPEH with a heartbeat of 60 bpm, (d) the photograph of two 1.0-mm-thick optimal soft-substrate sandwich FPEHs attached to the artificial diaphragm, symmetrically, (e) output voltages of the two FPEHs with the breath of ~0.5 Hz, (f) the photograph of the 1.0-mm-thick optimal soft-substrate sandwich FPEH installed on the tail of a grass fish. The output voltages as the fish (g) rested, (h) swam, and (i) struggled and escaped, (j) the 0.6-mm-thick optimal soft-substrate sandwich FPEH pasted on the artificial bird, and (k) the output voltages when the bird took off, climbed, cruised, and landed. All of the FPEHs in the figure are in the size of 3 cm × 6 cm.

The wearable and implantable electronics for the animals, named "electronic tags," have a strict weight limit [36], allowing only very small batteries. Harvesting energy directly from the animals, such as swimming fish and flying birds, could power these devices and extend their lifespan. A stretchable package made from polyurethane fabrics was used to install the 1.0-mm-thick optimal soft-substrate sandwich FPEH to the tail of a grass fish, as shown in Fig. 4(f). The output voltages as the fish rested, swam, struggled, and escaped were measured by the 10-MΩ-resistance voltmeter and shown in Figs. 4(g)–4(i), respectively. The animal experiments were approved by the Animal Care & Welfare Committee of the Institute of Mechanics, Chinese Academy of Sciences (No.

202203). In addition, the 0.6-mm-thick optimal soft-substrate sandwich FPEH was attached to an artificial flapping-wing bird to illustrate the ability to harvest energy from the flying bird, as shown in Fig. 4(f). The output voltages of the 0.6-mm-thick optimal soft-substrate sandwich FPEH, measured by the 10-MΩ-resistance voltmeter, as the bird took off, climbed, cruised, and landed were shown in Fig. 4(k).

In addition to the optimal structural design, we believe that to realize the above practical applications, the energy harvesting system requires the following performances as well: (1) high-performance piezoelectric materials with low mechanical stiffness, high piezoelectric constant, and high fatigue properties: this helps to

generate sufficient electrical energy with a long operating time of several years; (2) high-efficient energy harvesting circuit: this helps to store and utilize as much of the electrical energy produced by the FPEH as possible; (3) design for robust and comfortable wearing: FPEH needs to be worn stably on the living subject for a long period and must not cause any discomfort or illness; (4) bio-compatibility and environmental friendliness: Long-term contact with living subjects requires all parts of the FPEH to be biocompatible or have robust biocompatible packaging. These needs are being addressed by our ongoing research to advance the practical application of FPEH.

3 Conclusion

In summary, a novel optimal soft-substrate sandwich FPEH is proposed with the design of sufficient length and optimized substrate Young's modulus. The systematic theoretical analysis based on the sandwich beam model with plane-strain assumption and soft substrate considering both bending and shear deformations and the one-way coupling of piezoelectric effect was conducted. It is found that length is a crucial parameter for the sandwich FPEH, which has been ignored in previous works. The results reveal the existence of the optimal Young's modulus of the soft substrate with sufficient length, which can decrease the mechanical stiffness greatly, maximize the energy efficiency, and remain the high areal output energy density. In addition, the insensitivity of the energy efficiency to the thickness of the optimal soft substrates allows adopting a thicker substrate for the higher areal output energy density. The optimal soft-substrate sandwich FPEH with ($\tilde{E}_{sub}/\tilde{E}_p = 0.011$, $h_{sub} = 1.018$ mm) is then designed and fabricated. Compared to a specific conventional hard-substrate FPEH ($\tilde{E}_{sub}/\tilde{E}_p = 1.05$ and $h_{sub} = 0.671$ mm), the optimal soft-substrate sandwich FPEH exhibits greatly improved performance with the areal output energy density increasing by 33%, the mechanical stiffness reducing by 51%, and the energy efficiency increasing by 177%, simultaneously. Our optimal design avoids the trade-off between these three parameters that would significantly limit the practicality of sandwich FPEH and have not been well addressed in previous works.

Finally, demonstrated applications of the optimal soft-substrate sandwich FPEHs to the heart, the diaphragm, the swimming fish, and the flying bird are then conducted to show the practical scenarios and feasibilities. Our optimal structural design of the sandwich FPEH is also expected for other types of mechanical energy harvesters with a similar laminated structure, such as triboelectric and magnetostrictive energy harvesters.

Author Contribution Statement

Q.L., S.L., and Y.S. conceived the concept. Q.L., S.L., L.Z., X.C., Y.L., and X.X. conducted the theoretical derivation, all the experiments, FEA, and discussed all the data. Q.L., S.L., L.Z., X.C., Y.L., and Y.S. prepared the manuscript. Members of the "CAS Interdisciplinary Innovation Team (JCTD-2020-03)," including Y.H., Y.C., Y.Z., C.H., Y.W., Y.Y., and Y.S. discussed all the data and revised the manuscript. Y.S. supervised the project.

Conflict of Interest

There are no conflicts of interest.

Data Availability Statement

The datasets generated and supporting the findings of this article are obtainable from the corresponding author upon reasonable request.

Appendix A: The Bending and Shear Strain of the Substrate

The displacement $u_x(x, z)$ and normal strain $\varepsilon_{xx}(x, z)$ along the x direction of the top and bottom piezoelectric films can be expressed by the horizontal displacement u, curvature κ_p, and membrane strain ε_p as

$$\begin{cases} u_x^{top}(x, z) = u - \dfrac{dw}{dx}\left(z + \dfrac{h_p + h_{sub}}{2}\right) \\ u_x^{bottom}(x, z) = -u - \dfrac{dw}{dx}\left(z - \dfrac{h_p + h_{sub}}{2}\right) \end{cases} \tag{A1}$$

and

$$\begin{cases} \varepsilon_{xx}^{top}(x, z) = \varepsilon_p - \kappa_p\left(z + \dfrac{h_p + h_{sub}}{2}\right) \\ \varepsilon_{xx}^{bottom}(x, z) = -\varepsilon_p - \kappa_p\left(z - \dfrac{h_p + h_{sub}}{2}\right) \end{cases} \tag{A2}$$

With the continuity at the interface between the substrate and the piezoelectric film, the displacement and normal strain of the top and bottom surface can be expressed as

$$\begin{cases} u_{sub}^{top} = u_{sub}|_{z=-h_{sub}/2} = u - \dfrac{dw}{dx}\dfrac{h_p}{2} \\ u_{sub}^{bottom} = u_{sub}|_{z=h_{sub}/2} = -u + \dfrac{dw}{dx}\dfrac{h_p}{2} \end{cases} \tag{A3}$$

and

$$\begin{cases} \varepsilon_{sub}^{top} = \varepsilon_{sub}|_{z=-h_{sub}/2} = \varepsilon_p - \dfrac{\kappa_p h_p}{2} \\ \varepsilon_{sub}^{bottom} = \varepsilon_{sub}|_{z=h_{sub}/2} = -\varepsilon_p + \dfrac{\kappa_p h_p}{2} \end{cases} \tag{A4}$$

with assumptions of the linear and constant distributions along the thickness direction for the bending strain and shear strain respectively, the bending and shear strain

$$\begin{cases} \varepsilon_{sub}(x, z) = \dfrac{\varepsilon_{sub}^{bottom} - \varepsilon_{sub}^{top}}{h_{sub}}z = \dfrac{(-2\varepsilon_p + \kappa_p h_p)z}{h_{sub}} \\ \gamma_{sub}(x, z) = \dfrac{dw}{dx} + \dfrac{du}{dz} = \dfrac{dw}{dx} + \left(-2u + h_p\dfrac{dw}{dx}\right)\dfrac{1}{h_{sub}} \end{cases} \tag{A5}$$

Appendix B: Expressions of Coefficients of the Mechanical Results

The expressions of coefficients of Eq. (10) are as follows:

$$
\begin{cases}
H_{w0} = \dfrac{rsL}{-3a(b-ce)^2 \tanh(sL) + rsL}, \quad H_{w1} = \dfrac{3as(b-ce)^2}{3a(b-ce)^2 \tanh(sL) - rsL}, \\[2ex]
H_{w2} = \dfrac{3csLb(ba+bc-2ace)}{6a(b-ce)^2 \tanh(sL) - 2rsL}, \quad H_{w3} = \dfrac{csb(ba+bc-2ace)}{-6a(b-ce)^2 \tanh(sL) + 2rsL} \\[2ex]
H_{w4} = \dfrac{3a(b-ce)^2}{-3a(b-ce)^2 \sinh(sL) + rsL \cosh(sL)}
\end{cases}
\tag{B1}
$$

$$
\begin{cases}
H_{u0} = -\dfrac{3sac(b-ce)(b-ae)}{b[rsL - 3a\tanh(sL)(b-ce)^2]}, \quad H_{u1} = \dfrac{3sacL(ba+bc-2ace)}{rsL - 3a\tanh(sL)(b-ce)^2}, \\[2ex]
H_{u2} = \dfrac{-3sac(ba+bc-2ace)}{2[rsL - 3a\tanh(sL)(b-ce)^2]}, \quad H_{u3} = \dfrac{3sac(b-ce)(b-ae)}{b[rsL\cosh(sL) - 3a\sinh(sL)(b-ce)^2]}
\end{cases}
\tag{B2}
$$

and

$$
\begin{cases}
r = [(L^2c+3)(b^2-2bce) + 3c^2e^2]a + (Lbc)^2 \\[2ex]
s = \dfrac{\sqrt{b}\sqrt{(a+c)b - 2ace}}{\sqrt{b^2 - ace^2}}
\end{cases}
\tag{B3}
$$

Appendix C: Piezoelectric Performance of the Sandwich FPEH

For the piezoelectric film with in-plane isotropic mechanical properties, the piezoelectric governing equations are

$$
\begin{Bmatrix} \varepsilon_{11} \\ \varepsilon_{22} \\ \varepsilon_{33} \\ 2\varepsilon_{23} \\ 2\varepsilon_{31} \\ 2\varepsilon_{12} \end{Bmatrix} =
\begin{bmatrix}
\frac{1}{E_p} & -\frac{\nu_p}{E_p} & -\frac{\nu_{p3}}{E_{p3}} & 0 & 0 & 0 \\[1ex]
-\frac{\nu_p}{E_p} & \frac{1}{E_p} & -\frac{\nu_{p3}}{E_{p3}} & 0 & 0 & 0 \\[1ex]
-\frac{\nu_{p3}}{E_p} & -\frac{\nu_{p3}}{E_p} & \frac{1}{E_{p3}} & 0 & 0 & 0 \\[1ex]
0 & 0 & 0 & \frac{1}{G_{p3}} & 0 & 0 \\[1ex]
0 & 0 & 0 & 0 & \frac{1}{G_{p3}} & 0 \\[1ex]
0 & 0 & 0 & 0 & 0 & \frac{2(1+\nu_p)}{E_p}
\end{bmatrix}
\begin{Bmatrix} \sigma_{11} \\ \sigma_{22} \\ \sigma_{33} \\ \sigma_{12} \\ \sigma_{23} \\ \sigma_{31} \end{Bmatrix}
+
\begin{bmatrix}
0 & 0 & d_{31} \\
0 & 0 & d_{32} \\
0 & 0 & d_{33} \\
0 & d_{15} & 0 \\
d_{15} & 0 & 0 \\
0 & 0 & 0
\end{bmatrix}
\begin{Bmatrix} E_1 \\ E_2 \\ E_3 \end{Bmatrix}
\tag{C1}
$$

and

$$
\begin{Bmatrix} D_1 \\ D_2 \\ D_3 \end{Bmatrix} =
\begin{bmatrix}
0 & 0 & 0 & 0 & d_{15} & 0 \\
0 & 0 & 0 & d_{15} & 0 & 0 \\
d_{31} & d_{32} & d_{33} & 0 & 0 & 0
\end{bmatrix}
\begin{Bmatrix} \sigma_{11} \\ \sigma_{22} \\ \sigma_{33} \\ \sigma_{23} \\ \sigma_{31} \\ \sigma_{12} \end{Bmatrix}
+
\begin{bmatrix}
k_{33} & 0 & 0 \\
0 & k_{33} & 0 \\
0 & 0 & k_{33}
\end{bmatrix}
\begin{Bmatrix} E_1 \\ E_2 \\ E_3 \end{Bmatrix}
\tag{C2}
$$

Considering the plane-strain condition $\varepsilon_{22} = 0$ and the traction-free condition on the surface of the FPEH $\sigma_{33} = 0$, Eq. (C1) can be simplified as

$$
\begin{cases}
\varepsilon_{11} = \dfrac{1}{E_p}\sigma_{11} - \dfrac{\nu_p}{E_p}\sigma_{22} + d_{31}E_3 \\[2ex]
0 = -\dfrac{\nu_p}{E_p}\sigma_{11} + \dfrac{1}{E_p}\sigma_{22} + d_{32}E_3
\end{cases}
\tag{C3}
$$

and rewrite into

$$
\begin{cases}
\varepsilon_{11} = \dfrac{1-\nu_p^2}{E_p}\sigma_{11} + (d_{31} + \nu_p d_{32})E_3 \\[2ex]
\sigma_{22} = \nu_p\sigma_{11} - E_p(d_{32}E_3)
\end{cases}
\tag{C4}
$$

Substitute (C4) into (C2), we have

$$
D_3 = \bar{e}\varepsilon_{11} + \bar{k}E_3
\tag{C5}
$$

where $\bar{e} = (d_{31} + \nu_p d_{32})\tilde{E}_p$ and $\bar{k} = k_{33} - \tilde{E}_p(d_{31} + \nu_p d_{32})^2 - E_p d_{32}^2$. Substitute the normal strain of the piezoelectric film Eq. (A2) into (C5),

we have

$$\begin{cases} D_3^{\text{top}} = \bar{e}\left[\varepsilon_{\text{p}} - \kappa_{\text{p}}\left(z + \dfrac{h_{\text{p}} + h_{\text{sub}}}{2}\right)\right] + \bar{k}E_3^{\text{top}} \\[2mm] D_3^{\text{bottom}} = \bar{e}\left[-\varepsilon_{\text{p}} - \kappa_{\text{p}}\left(z - \dfrac{h_{\text{p}} + h_{\text{sub}}}{2}\right)\right] + \bar{k}E_3^{\text{bottom}} \end{cases} \quad \text{(C6)}$$

for the top and bottom piezoelectric film, respectively. There are no free charges in the piezoelectric film and the voltage on the electrode is equal everywhere

$$\frac{\partial D_3}{\partial z} = 0, \ \frac{\partial V}{\partial x} = 0 \quad \text{(C7)}$$

Integrated Eq. (C6) in the z-direction with Eq. (C7), we have

$$\begin{cases} D_3^{\text{top}} = \bar{e}\varepsilon_{\text{p}} - \dfrac{\bar{k}}{h_{\text{p}}}V_{\text{top}} \\[2mm] D_3^{\text{bottom}} = \bar{e}(-\varepsilon_{\text{p}}) - \dfrac{\bar{k}}{h_{\text{p}}}V_{\text{bottom}} \end{cases} \quad \text{(C8)}$$

where $V_{\text{top}} = -\int_{-h_{\text{p}}-h_{\text{sub}}/2}^{-h_{\text{sub}}/2} E_3^{\text{top}}\mathrm{d}z$ and $V_{\text{bottom}} = -\int_{h_{\text{sub}}/2}^{h_{\text{p}}+h_{\text{sub}}/2} E_3^{\text{bottom}}\mathrm{d}z$.

Integrate Eq. (C8) over the surface area, we have

$$\begin{cases} 2W\bar{e}u|_{x=L} = 2W\int_0^L D_3^{\text{top}}\mathrm{d}x + \bar{k}\dfrac{2WL}{h_{\text{p}}}V_{\text{top}} \\[2mm] 2W\bar{e}u|_{x=L} = -\left(2W\int_0^L D_3^{\text{bottom}}\mathrm{d}x + \bar{k}\dfrac{2WL}{h_{\text{p}}}V_{\text{bottom}}\right) \end{cases} \quad \text{(C9)}$$

where $u|_{x=L} = (H_{u0} + H_{u1}L + H_{u2}L^2)w_0$, and, for both equations, the first term presents the charges generated by the piezoelectric effect, the second term presents the free charges on the electrode and equals zero under the ideal open-circuit condition, and the third term presents the net charges on the electrode. By connecting the two inner electrodes of the FPEH as a pair and the two outer electrodes as a pair, the two piezoelectric films are electrically connected in parallel, and a total expression is expressed as

$$4W\bar{e}(H_{u0} + H_{u1}L + H_{u2}L^2)w_0 = \bar{k}\frac{4WL}{h_{\text{p}}}V + 4W\int_0^L D_3\mathrm{d}x \quad \text{(C10)}$$

where $C_{\text{p}} = C_{\text{p\_t}} + C_{\text{p\_b}} = 4\bar{k}WL/h_{\text{p}}$ is the total capacitance of the two piezoelectric films in parallel. Substituting $4W\int_0^L D_3\mathrm{d}x = 0$ for the open-circuit condition in Eq. (C10), the open-circuit output voltage Eq. (15) and the output electric energy, which is stored in the capacitance of the FPEH, $U_{\text{total\_output}} = C_{\text{p}}V^2/2$ can be obtained.

Appendix D: Theoretical and Finite Element Analysis Results of the Deformation of the Sandwich FPEH

The governing equations for u and w of the FPEH (Eq. (7)) and the boundary conditions (Eq. (8)) were obtained by the variation of the total elastic energy (Eq. (6)), which was conducted by hand. The coefficients of the governing equation Eq. (7) are carefully sorted to obtain a general solution of the simplest possible form. Equation (7) was then solved with the boundary conditions Eq. (8) using the commercial software Maple (Maplesoft, Waterloo, Canada). Particular solutions were obtained by the command "*dsolve*". All results of calculations with specific parameters were carried out using the commercial software MATLAB (MathWorks, Natick, MA). All of the original files can be requested by contacting the corresponding author.

The deformation of the sandwich FPEH with various substrate moduli was performed employing the commercial software ABAQUS (SIMULIA, Yvelines, France). Similar to our previous works [32,33], $2L$, h_{p}, h_{sub}, E_{p}, E_{sub}, ν_{p}, and ν_{sub} were consistent with the theoretical results, but the width W was set to 0.05 mm. The displacement along the y-axis was set to zero to meet the plane-

strain condition. The simply supported boundary conditions were set at both ends of the lower surface of the sandwich FPEH, with a displacement load of 5 mm set at the middle ($x=0$) of the upper surface of the sandwich FPEH. Without any assumption of the plane section or shear lag, the 20-node quadratic brick element C3D20R was utilized for both the substrate and the piezoelectric film. The numbers of meshes for two piezoelectric layers and the substrate layer were all 300 in the length direction, nine in the thickness direction, and one in the width direction.

Appendix E: Fabrication and Experimental Process of the FPEH

All of the piezoelectric films were made by the 55 μm thick and surface aluminized PVDF films purchased from the Jinzhou Kexin Dianzi Cailiao Co., Ltd., Jinzhou, China. PU and PET sheets of different thicknesses were purchased for the soft and hard substrates, respectively. A pair of three-point bending fixtures was 3D printed with acrylonitrile butadiene styrene. The programmable mechanical testing machine (ZQ-990A, ZHIQU, Dongguan, China), 200-TΩ-resistance voltmeter (Keithley 6517B, Tektronix, Beaverton, OR) with 360 pF capacitance, and 10-MΩ-resistance voltmeter (Keysight DAQ970A, Santa Rosa, CA) were used for the experiments.

Appendix F: Output Voltages of the Sandwich FPEH Measured by the Voltmeter With the Finite Resistance and Capacitance

When connected the FPEH to an external circuit with resistance and capacitance, as shown in Fig. 3(c), the term $4W\int_0^L D_3\mathrm{d}x$ is not equal to zero anymore but represents the free charges flow in from and flow out to the external circuit. Take the derivative of Eq. (C10) with time t, the flow of charges, i.e., the current, can be obtained

$$4W\bar{e}(H_{u0} + H_{u1}L + H_{u2}L^2)\frac{\mathrm{d}}{\mathrm{d}t}w_0 = C_{\text{P}}\frac{\mathrm{d}V}{\mathrm{d}t} + (I_{\text{R\_CPEH}} + I_{\text{C\_V}} + I_{\text{R\_V}}) \quad \text{(F1)}$$

Based on Ohm's law and the I–V relationship of the capacitance, the external current can be expressed as

$$I_{\text{R\_CPEH}} + I_{\text{R\_V}} + I_{\text{C\_V}} = \left(\frac{1}{R_{\text{P\_t}}} + \frac{1}{R_{\text{p\_b}}}\right)V + \frac{V}{R_{\text{V}}} + C_{\text{V}}\frac{\mathrm{d}V}{\mathrm{d}t} \quad \text{(F2)}$$

Substitute Eq. (F2) into Eq. (F1), we have the differential equation for the output voltage

$$C\frac{\mathrm{d}V}{\mathrm{d}t} + \frac{V}{R} = 4W\bar{e}(H_{u0} + H_{u1}L + H_{u2}L^2)\frac{\mathrm{d}}{\mathrm{d}t}w_0 \quad \text{(F3)}$$

where C and R are the total capacitance and resistance of the circuit. Equation (21) can be obtained by solving Eq. (F3) with the initial condition $V(t=0) = 0$.

Appendix G: Modified Results for the 1.0-mm-Thick Optimal Soft-Substrate Sandwich FPEH With Bonding Layers

With the thickness non-negligible bonding layer, the piezoelectric films are not located at the central plane of the top and bottom surface hard layer but are off by a distance of $h_{\text{bond}}/2$, as shown in Fig. S3 available in the Supplemental Materials. Assume that the bonding layer has the same plane-strain Young's modulus as the piezoelectric film, within the mechanical equations, the bilayer of the bonding layer and the piezoelectric film can be considered as one hard surface layer with thickness $h_{\text{p}} + h_{\text{bond}}$. The horizontal displacement u is defined at the central line of the hard surface layer, with the results of membrane strain $\varepsilon_{\text{c}} = \mathrm{d}u/\mathrm{d}x$ and curvature $\kappa_{\text{c}} = \mathrm{d}^2w/\mathrm{d}x^2$. And then, the

mechanical results can be yielded by replacing the term h_p with the total thickness of the hard surface layer $h_p + h_{bond}$ when calculating the displacement w and u Eq. (10), the membrane strain and curvature ε_c and κ_c, the normal and shear strain of the substrate ε_{sub} and γ_{sub} (Eq. (A5)), and the elastic energy $U_{elastic}$ (Eq. (13)). Specifically, the coefficients a, b, c, and e, as well as the normal and shear strain of the substrate should be modified as

$$
\begin{cases}
a = 6(1 - \nu_{sub})[1 + (h_p + h_{bond})/h_{sub}]^2 / \{(h_p + h_{bond})^2[2\tilde{E}_p(h_p + h_{bond})/(\tilde{E}_{sub}h_{sub}) + 1]\} \\
b = -12(1 - \nu_{sub})[1 + (h_p + h_{bond})/h_{sub}]/\{h_{sub}(h_p + h_{bond})^2[2\tilde{E}_p(h_p + h_{bond})/(\tilde{E}_{sub}h_{sub}) + 1]\} \\
c = 6(1 - \nu_{sub})/\{h_{sub}^2[6\tilde{E}_p(h_p + h_{bond})/(\tilde{E}_{sub}h_{sub}) + 1]\} \\
e = -2/\{(h_p + h_{bond})[2\tilde{E}_p(h_p + h_{bond})/(\tilde{E}_{sub}h_{sub}) + 1]\}
\end{cases}
\tag{G1}
$$

and

$$
\begin{aligned}
\varepsilon_{sub} &= [-2\varepsilon_p + \kappa_p(h_p + h_{bond})]z/h_{sub} \\
\gamma_{sub} &= dw/dx + [-2u + (h_p + h_{bond})dw/dx]/h_{sub}
\end{aligned}
\tag{G2}
$$

Due to the deviation of the piezoelectric film from the central line of the hard surface layer, the membrane strain and displacement of the piezoelectric film are

$$
\begin{cases}
\varepsilon_p = \varepsilon_c + \kappa_c \dfrac{h_{bond}}{2} \\
u_p = u + \dfrac{dw}{dx}\dfrac{h_{bond}}{2}
\end{cases}
\tag{G3}
$$

Substitute Eq. (10) into Eq. (G3), and let $x = L$, we have

$$
u_p|_{x=L} = \left[\left(H_{u0} + \frac{1}{2}h_b H_{w1}\right) + (H_{u1} + h_b H_{w2})L + \left(H_{u2} + \frac{3}{2}h_b H_{w3}\right)L^2\right]w_0
\tag{G4}
$$

Thus, the modified coefficients of the displacement of the piezoelectric films can be obtained

$$
H_{u0}^m = H_{u0} + \frac{1}{2}h_b H_{w1},\ H_{u1}^m = H_{u1} + h_b H_{w2},\ \text{and}\ H_{u2}^m = H_{u2} + \frac{3}{2}h_b H_{w3}
\tag{G5}
$$

The coefficients H_{u0}, H_{u1}, and H_{u2}, substituted into the piezoelectric and electric equations Eqs. (17)–(21), should be modified as Eq. (G5). The bonding layers have no piezoelectric effect, so the thickness of piezoelectric film h_p remains unchanged in the piezoelectric and electric equations.

References

[1] Yacoub, M. H., and McLeod, C., 2018, "The Expanding Role of Implantable Devices to Monitor Heart Failure and Pulmonary Hypertension," Nat. Rev. Cardiol., 15(12), pp. 770–779.

[2] Song, E., Li, J., Won, S. M., Bai, W., and Rogers, J. A., 2020, "Materials for Flexible Bioelectronic Systems as Chronic Neural Interfaces," Nat. Mater., 19(6), pp. 590–603.

[3] Wang, X., Shi, Y., Yang, P., Tao, X., Li, S., Lei, R., Liu, Z., Wang, Z. L., and Chen, X., 2022, "Fish-Wearable Data Snooping Platform for Underwater Energy Harvesting and Fish Behavior Monitoring," Small, 18(10), p. 2107232.

[4] Mancuso, K. A., Fylling, M. A., Bishop, C. A., Hodges, K. E., Lancaster, M. B., and Stone, K. R., 2021, "Migration Ecology of Western Gray Catbirds," Movement Ecol., 9(1), p. 10.

[5] Zheng, Q., Tang, Q., Wang, Z. L., and Li, Z., 2021, "Self-Powered Cardiovascular Electronic Devices and Systems," Nat. Rev. Cardiol., 18(1), pp. 7–21.

[6] Hussey, N. E., Kessel, S. T., Aarestrup, K., Cooke, S. J., Cowley, P. D., Fisk, A. T., Harcourt, R. G., et al., 2015, "Aquatic Animal Telemetry: A Panoramic Window Into the Underwater World," Science, 348(6240), p. 1255642.

[7] Ahn, Y., Song, S., and Yun, K.-S., 2015, "Woven Flexible Textile Structure for Wearable Power-Generating Tactile Sensor Array," Smart Mater. Struct., 24(7), p. 075002.

[8] Chen, D., Chen, K., Brown, K., Hang, A., and Zhang, J. X. J., 2017, "Liquid-Phase Tuning of Porous PVDF-TrFE Film on Flexible Substrate for Energy Harvesting," Appl. Phys. Lett., 110(15), p. 153902.

[9] Dagdeviren, C., Yang, B. D., Su, Y., Tran, P. L., Joe, P., Anderson, E., Xia, J., et al., 2014, "Conformal Piezoelectric Energy Harvesting and Storage From Motions of the Heart, Lung, and Diaphragm," Proc. Natl. Acad. Sci. U. S. A., 111(5), pp. 1927–1932.

[10] Hyeon, D. Y., and Park, K.-I., 2019, "Piezoelectric Flexible Energy Harvester Based on BaTiO$_3$ Thin Film Enabled by Exfoliating the Mica Substrate," Energy Technol., 7(10), p. 1900638.

[11] Khan, M. B., Kim, D. H., Han, J. H., Saif, H., Lee, H., Lee, Y., Kim, M., et al., 2019, "Performance Improvement of Flexible Piezoelectric Energy Harvester for Irregular Human Motion With Energy Extraction Enhancement Circuit," Nano Energy, 58, pp. 211–219.

[12] Hwang, G.-T., Park, H., Lee, J.-H., Oh, S., Park, K.-I., Byun, M., Park, H., et al., 2014, "Self-Powered Cardiac Pacemaker Enabled by Flexible Single Crystalline PMN-PT Piezoelectric Energy Harvester," Adv. Mater., 26(28), pp. 4880–4887.

[13] Li, N., Yi, Z., Ma, Y., Xie, F., Huang, Y., Tian, Y., Dong, X., et al., 2019, "Direct Powering a Real Cardiac Pacemaker by Natural Energy of a Heartbeat," ACS Nano, 13(3), pp. 2822–2830.

[14] Yang, R., Qin, Y., Dai, L., and Wang, Z. L., 2009, "Power Generation With Laterally Packaged Piezoelectric Fine Wires," Nat. Nanotechnol., 4(1), pp. 34–39.

[15] Sun, R., Zhang, B., Yang, L., Zhang, W., Farrow, I., Scarpa, F., and Rossiter, J., 2018, "Kirigami Stretchable Strain Sensors With Enhanced Piezoelectricity Induced by Topological Electrodes," Appl. Phys. Lett., 112(25), p. 251904.

[16] Dong, L., Closson, A. B., Oglesby, M., Escobedo, D., Han, X., Nie, Y., Huang, S., Feldman, M. D., Chen, Z., and Zhang, J. X. J., 2019, "In Vivo Cardiac Power Generation Enabled by an Integrated Helical Piezoelectric Pacemaker Lead," Nano Energy, 66, p. 104085.

[17] Dong, L., Wen, C., Liu, Y., Xu, Z., Closson, A. B., Han, X., Escobar, G. P., et al., 2019, "Piezoelectric Buckled Beam Array on a Pacemaker Lead for Energy Harvesting," Adv. Mater. Technol., 4(1), p. 1800335.

[18] Jeong, C. K., Baek, C., Kingon, A. I., Park, K.-I., and Kim, S.-H., 2018, "Lead-Free Perovskite Nanowire-Employed Piezopolymer for Highly Efficient Flexible Nanocomposite Energy Harvester," Small, 14(19), p. 1704022.

[19] Park, K.-I., Son, J. H., Hwang, G.-T., Jeong, C. K., Ryu, J., Koo, M., Choi, I., et al., 2014, "Highly-Efficient, Flexible Piezoelectric PZT Thin Film Nanogenerator on Plastic Substrates," Adv. Mater., 26(16), pp. 2514–2520.

[20] Kim, D. H., Shin, H. J., Lee, H., Jeong, C. K., Park, H., Hwang, G.-T., Lee, H.-Y., et al., 2017, "In Vivo Self-Powered Wireless Transmission Using Biocompatible Flexible Energy Harvesters," Adv. Funct. Mater., 27(25), p. 1700341.

[21] Dagdeviren, C., Li, Z., and Wang, Z. L., 2017, "Energy Harvesting From the Animal/Human Body for Self-Powered Electronics," Annu. Rev. Biomed. Eng., 19(1), pp. 85–108.

[22] Jung, W.-S., Lee, M.-J., Kang, M.-G., Moon, H. G., Yoon, S.-J., Baek, S.-H., and Kang, C.-Y., 2015, "Powerful Curved Piezoelectric Generator for Wearable Applications," Nano Energy, 13, pp. 174–181.

[23] Fu, J., Hou, Y., Zheng, M., and Zhu, M., 2020, "Flexible Piezoelectric Energy Harvester With Extremely High Power Generation Capability by Sandwich Structure Design Strategy," ACS Appl. Mater. Interfaces, 12(8), pp. 9766–9774.

[24] Petritz, A., Karner-Petritz, E., Uemura, T., Schäffner, P., Araki, T., Stadlober, B., and Sekitani, T., 2021, "Imperceptible Energy Harvesting Device and Biomedical Sensor Based on Ultraflexible Ferroelectric Transducers and Organic Diodes," Nat. Commun., 12(1), p. 2399.

[25] Yaqoob, U., Habibur, R. M., Sheeraz, M., and Kim, H. C., 2019, "Realization of Self-Poled, High Performance, Flexible Piezoelectric Energy Harvester by Employing PDMS-rGO as Sandwich Layer Between P(VDF-TrFE)-PMN-PT Composite Sheets," Compos. Part B: Eng., 159, pp. 259–268.

[26] Li, L., Lin, H., Qiao, S., Zou, Y., Danto, S., Richardson, K., Musgraves, J. D., Lu, N., and Hu, J., 2014, "Integrated Flexible Chalcogenide Glass Photonic Devices," Nat. Photonics, 8(8), pp. 643–649.

[27] Allen, H. G., 1969, Analysis and Design of Structural Sandwich Panels, 1st ed., Pergamon Press, Oxford, New York, pp. 1–7.

[28] Jo, W., Lee, H., Lee, Y., Bae, B.-S., and Kim, T.-S., 2021, "Controlling Neutral Plane of Flexible Substrates by Asymmetric Impregnation of Glass Fabric for Protecting Brittle Films on Foldable Electronics," Adv. Eng. Mater., 23(6), p. 2001280.

[29] Shi, Y., Rogers, J. A., Gao, C., and Huang, Y., 2014, "Multiple Neutral Axes in Bending of a Multiple-Layer Beam With Extremely Different Elastic Properties," ASME J. Appl. Mech., 81(11), p. 114501.

[30] Lu, N., Yang, S., and Qiao, S., 2014, "Mechanics of Flexible Electronics and Photonics Based on Inorganic Micro- and Nanomaterials," Conference on Micro- and Nanotechnology Sensors, Systems, and Applications VI, Baltimore, MD, May 5–9, Article No. 90831J.

[31] Lee, T.-I., Jo, W., Kim, W., Kim, J.-H., Paik, K.-W., and Kim, T.-S., 2019, "Direct Visualization of Cross-Sectional Strain Distribution in Flexible Devices," ACS Appl. Mater. Interfaces, **11**(14), pp. 13416–13422.

[32] Li, S., Su, Y., and Li, R., 2016, "Splitting of the Neutral Mechanical Plane Depends on the Length of the Multi-Layer Structure of Flexible Electronics," Proc. R. Soc. A: Math., Phys. Eng. Sci., **472**(2190), p. 20160087.

[33] Su, Y., Li, S., Huan, Y., Li, R., Zhang, Z., Joe, P., and Dagdeviren, C., 2017, "The Universal and Easy-to-Use Standard of Voltage Measurement for Quantifying the Performance of Piezoelectric Devices," Extreme Mech. Lett., **15**, pp. 10–16.

[34] Li, S., Liu, X., Li, R., and Su, Y., 2017, "Shear Deformation Dominates in the Soft Adhesive Layers of the Laminated Structure of Flexible Electronics," Int. J. Solids Struct., **110**, pp. 305–314.

[35] Cohrs, N. H., Petrou, A., Loepfe, M., Yliruka, M., Schumacher, C. M., Kohll, A. X., Starck, C. T., et al., 2017, "A Soft Total Artificial Heart-First Concept Evaluation on a Hybrid Mock Circulation," Artif. Organs, **41**(10), pp. 948–958.

[36] Geen, G. R., Robinson, R. A., and Baillie, S. R., 2019, "Effects of Tracking Devices on Individual Birds—A Review of the Evidence," J. Avian Biol., **50**(2), p. e01823.